

Three-dimensional comparison of fractal and homogeneous cloud structure

Ben Hood^{1,2}, Kenny Wood¹, Sara Seager², Andrew Cameron¹

¹*School of Physics & Astronomy, University of St Andrews, North Haugh, St Andrews, Fife KY16 9SS, Scotland*

²*Department of Terrestrial Magnetism, Carnegie Institution of Washington 5241 Broadbranch Road, Washington, DC 20015*

14 April 2006

ABSTRACT

We present results of our Monte Carlo based radiation transfer simulations. In anticipation of using this code to simulate extrasolar planetary atmospheres, we have tested varying single scattering albedos, phase functions, fractal distributions of clouds, optical depths, and bottom layers. We have found that several factors significantly influence the eventual overall albedo of a planet, especially the fractal distribution of the mass, which can reduce the albedo of a planet by nearly 60%. This work will help explain why the extrasolar planets are so dark.

Key words: methods: radiation transfer simulations

1 INTRODUCTION

In spite of intense effort, observers have, thus far, been unable to detect stellar light reflected from the atmosphere of any extrasolar planets. Cameron et al. (1999) and Charbonneau et al. (1999) have developed systems to theoretically tease apart the spectral lines of an extrasolar planet from the lines of the parent star, but they have been unable to definitively detect the faint signature. A detection by Cameron et al. (1999) was unverifiable in the observing season following the detection (Cameron et al. 2001). However, through their subsequent work, they have been able to set the upper geometric albedo limit of the planet at 0.39 (Leigh et al. 2003). Similar work has set an albedo limit on HD 209458 of 0.25 in the MOST bandpass (Rowe et al. 2006).

Charbonneau et al. (2005) and Deming et al. (2005) have detected reprocessed emissions from extrasolar planets with Spitzer, but both of these detections are of infrared radiation, rather than optical radiation, and in both cases the total radiation of the planet-star system is measured, but the specific photons from the planet cannot be isolated.

Thus, we aim to understand why the extrasolar planets we are observing are so dark, such that they don't reflect much of their stellar incident light. To that end, we have developed a three-dimensional model of an extrasolar planetary atmosphere.

We would like to specifically pursue the three-dimensional and fractal effects of our simulated atmosphere. We are motivated in this regard by atmospheric sciences, in which Lovejoy (1982) showed that clouds are fractal in na-

ture, at least horizontally. Additionally, Kuchinke, Fienberg and Nunez (2004) showed that a three-dimensional fractal cloud simulation results in a more accurate representation of real clouds than a plane-parallel homogenous simulation. Though we lack the large amount of data of atmospheric scientists studying the Earth, some of these advances are applicable to extrasolar planetary atmospheric simulations.

2 SIMULATION CODE

2.1 Introduction and history

Radiation transfer is the study of light traversing a medium. Exact solutions exist for some simple cases of radiation transfer. However, our focus is to explore a clumpy medium with multiple types of scattering species, which poses challenges to solve analytically. Monte Carlo simulations are better suited to this type of problem. It is called Monte Carlo because it is based on chance, just like the casino tables of Monte Carlo. The radiation in our simulations behaves according to probability: many photons go in the direction that is most probable, and only a few photons go in the direction that is least probable. If we only observed one photon going through our medium, then it would not give us a good idea of how photons act, because it could take a very unlikely path. However, we use 1,000,000 photons and watch how all of them go through the medium, which gives us a good idea of how all photons will act.

Our three-dimensional code simulates the radiation

Table 1. Fixed Model Parameters

Number of Scattering Species
Exponential Atmosphere Scale Height
Number of Photon Packets
Cartesian Resolution (# of x,y,z cells)
Tiling Resolution (# of surface cells)
Viewing Resolution
Dense, Transparent, or Lambert bottom layer
Three-Dimensional Fractal Dimension

Table 2. Scattering Species Parameters

Scattering Phase Function
Fractal or Smooth Mass Distribution
Cloud Coverage
Optical Depth
Mass Fraction of Total
Single Scattering Albedo
Upper and Lower Cloud Height Limits

transfer in an extrasolar planetary atmosphere. It is a modified form of the three-dimensional Monte Carlo scattering code used by Wood and Reynolds (1999). The medium through which the photons travel is mass distributed throughout a grid. Photon packets are emitted, travel some distance and then are either absorbed or scattered in some direction. We record the direction and number of photon packets scattered. In comparison to the code which was used in Wood and Reynolds (1999), we have made the simulations semi-infinite, meaning photons leaving the side of the simulation come back in the other side. We have also added multiple scattering species support, and used the output from this code to build a spherical model of the exoplanet as a whole.

2.2 Code structure

Our simulation of an entire extrasolar planet atmosphere is actually an integration of many small simulations of cubes of atmosphere on the extrasolar planet. We will first describe the small simulations, which we call Cartesian simulations, in 2.2.1. We will then describe how we integrate the small simulations to build the entire planet in 2.2.2. This is referred to as “tiling,” because it is similar to tiling the Cartesian cubes onto the surface of a sphere to make the planet atmosphere.

2.2.1 Cartesian Grid

Conceptually, our Cartesian grid simulation is like a small patch of atmosphere on the surface of our entire extrasolar planet simulation. It is approximated as a cube, and might be 100 miles tall, 100 miles wide, and 100 miles deep—depending on where it is on the surface of our cube, the star light will illuminate it at some specific angle. We simulate these small cubes—instead of simulating the entire sphere—because many places on the planet have the same illumination angle, and can be represented by the same cube. We only have to run the simulation once in order to know how a

multitude of cubes of atmosphere will react (all those cubes with the same illumination angle).

The specifics of the simulation code are presented in Wood and Reynolds (1999), where it was used to model the diffuse $H\alpha$ galactic background. The simulation code is a Cartesian grid with semi-infinite boundaries.

One of the most important characteristics of our simulation code is how we distribute the mass in our atmosphere. First, we choose whether or not we want all the mass distributed uniformly. If we choose to make it uniform, it is similar to a plane-parallel homogenous simulation. If we choose to make our mass “clumpy,” or not uniform, then we use a hierarchical distribution algorithm presented by Elmegreen (1997). Our specific implementation of the fractal distribution is detailed in Wood et al. (2005), and is summarized here. We use five levels, and at the first, top level we randomly choose N points with x , y , and z coordinates in the range (0,1). At each subsequent level we choose 32 random points around each of the points chosen at the previous level. In the end, we have placed all the points into different grid cells.

The mass assigned to each grid cell is proportional to the number of points cast into the cell. The optical depth we assign to fractally distributed mass is the optical depth the mass would have if smoothly distributed over the entire grid, i.e. we aren’t adding or taking away mass, we are just rearranging it. Thus, some of the specific column integrations have optical depths greater than the equivalent smooth model, and some have depths less than the equivalent smooth model. We show various column integrations in figure 1 from the fractal distribution. Figure 2 shows the same data as fractal seed = 32 from figure 1 but with a voxel projection, to exhibit the distribution of mass throughout the three-dimensional space.

Our models use a three-dimensional fractal dimension of 2.6. Sánchez, Alfaro, Pérez (2005) show that this value roughly corresponds to a projected two-dimensional area-perimeter dimension of 1.36. This value is very close to the area-parimeter dimension for rain and cloud areas observed by Lovejoy (1982).

The code builds a mass distribution grid for every scattering species. We can choose as many scattering species as computational power allows, and can independently assign an optical depth, single scattering albedo, or phase function to each different scattering species. Table 2 lists all possible scattering species parameters. Thus, we have one Cartesian grid with multiple scattering species in each grid cell.

The injection of around 1,000,000 photon packets into the simulation results in a good signal to noise ratio. For each photon packet the code calculates the path, determining if it will scatter or be absorbed and allowing it to exit the simulation at one of the boundaries of the Cartesian grid. Since we are working with a semi-infinite simulation, the photons which exit the sides of the grid are recreated on the opposite side of the grid. When photons escape the grid (out the top or the bottom), they are binned according the direction from which they exited, in equal solid angle bins.

We thus build a statistical map of what direction the photons are exiting the grid. Figure 3 shows the output of this Cartesian simulation, which reports the levels of photons in each direction of ϕ and μ .

By varying the incident angle of radiation, we can simu-

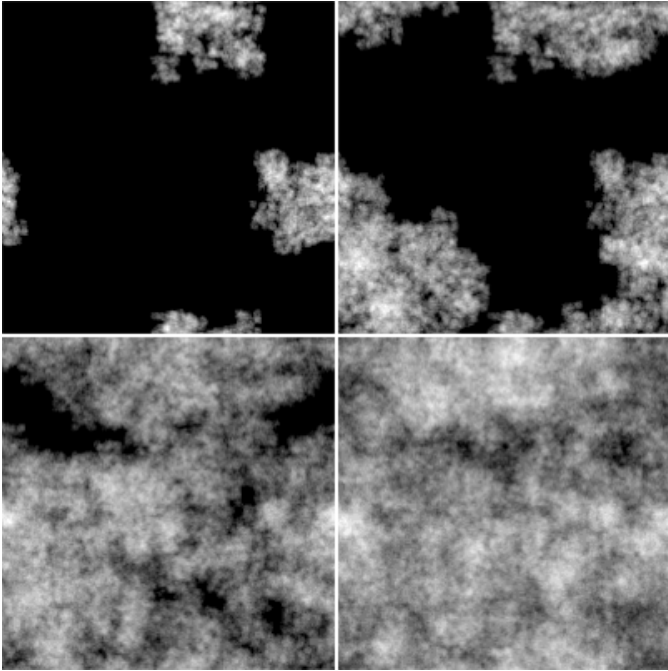


Figure 1. *Varied Fractal Distribution.* Each cell shows the column integrations for each of four fractally distributed simulations. Left to right and top to bottom: fractal seed=2 (which approximately corresponds to 15% cloud coverage), fractal seed = 8 (or 45% coverage), fractal seed = 32 (or 92% coverage), and fractal seed = 128 (or 100% coverage).

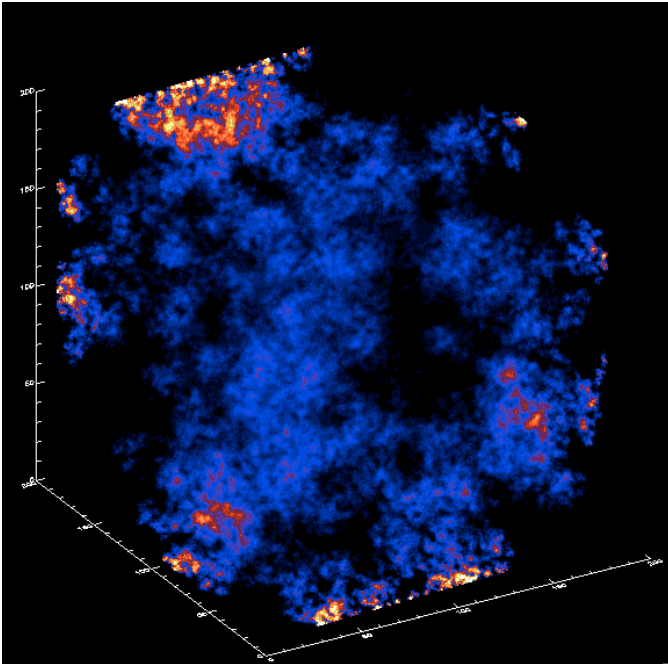


Figure 2. *Voxel Projection of Mass Distribution.* This is the distribution of mass from fractal seed = 32, also shown in column integration form in figure 1. This representation, a voxel projection, highlights the distribution of mass throughout the three-dimensional space of the simulation.

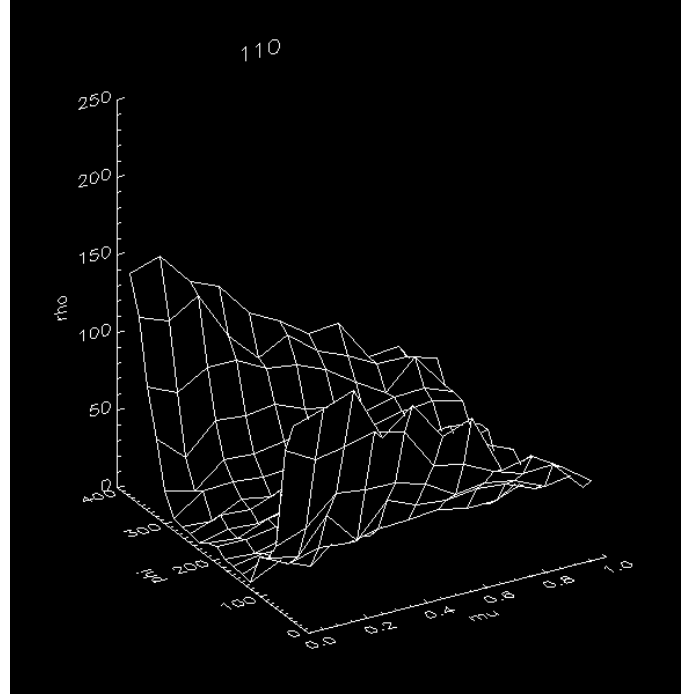


Figure 3. *Photon Packets per Solid Angle Bin.* In this graph, we present the results of one of our Cartesian simulations. This particular simulation has light incident on the surface of 110° (measured from the normal into the plane). At each ϕ and μ , we have a particular number of photon packets (ρ), depicted on the z axis. A Lambert sphere, for comparison, would have all ρ values of 500, within photon noise.

late all the different small patches of atmosphere. This provides the necessary information for the tiling code, discussed in section 2.2.2. We will typically run Cartesian simulations using incidence angles of 0° to 85° (measured from the normal from the plane of the surface) in 5° increments. The results from these simulations are then integrated into the tiling program.

2.2.2 Tiling

In order to turn the many small Cartesian simulations into a representation of the entire planet, we “tile” the small simulations onto a sphere. We then add up all the different small contributions to reflected light in order to know the total reflectivity of the sphere. A convenient analogy is a mirror disco ball. Our small Cartesian simulations tell us how reflective each piece of mirror is on the ball, and then by tiling, we know how reflective the entire ball is.

The Cartesian simulation allows us to specify the incident angle of radiation and then compare that angle to the number of photons coming out in each direction around the grid. We specify the resolution of the photon bins as 20 bins in μ and 20 bins in ϕ , giving 400 total bins. To normalize for the number of bins we choose, the photons in each bin are divided by a factor of $N_{ph}/((N_\mu/2) \times N_\phi)$, where N_{ph} is the number of photons, and N_μ and N_ϕ are the number of bins we choose. If the surface scatters all radiation incident on it with equal probability in all outward directions, then we will get a value of one in all directions.

Thus, the Cartesian simulations allow us to specify an incident angle of radiation, an emergent angle of scattered radiation and find the flux compared to a isotropically scattering surface. Using equation 9.8 from Sobolev (1975)

$$H(\alpha) = \int_{\alpha-\pi/2}^{\pi/2} \cos(\alpha-\omega) \cos\omega d\omega \int_0^{\pi/2} \rho(\eta, \zeta, \phi) \cos^3\psi d\psi(1)$$

we can find the $H(\alpha)$, the radiation flux emerging from a planet with respect to the planetary phase α . In this equation η is cosine of the angle of emergence with respect to the outward normal, ζ is the cosine of the angle of incidence with respect to the outward normal, ϕ is the azimuthal angle between those two angles. The planetocentric coordinates of latitude and longitude are represented by ψ and ω . Finally, ρ is the reflection coefficient, or the flux scattered in a particular direction from the surface compared to an isotropically scattering surface. For a more complete treatment of using the reflection coefficient to determine the total flux of the planet, see Sudarsky et al. (2005) or the original Sobolev (1975).

2.3 Testing and Code Limits

2.3.1 Comparison to Lambert Sphere

In order to test our code, we have reproduced the phase function of a Lambert sphere. In figure 4, we compare our results with an independent calculation of a Lambert's sphere, or a sphere with an isotropically scattering surface. It is a well know result that a Lambert surface will result in a reflected flux of:

$$\Phi_{sphere} = \frac{2}{3}\pi a I_0 r^2 \quad (2)$$

We find a satisfying agreement of our simulation results and the Lambert sphere. There is a slight discrepancy because of the coarseness of our numerical integration. If we increase the resolution of the integration by 10, our simulation results are almost exactly the results from the independently calculated Lambert sphere, but we have determined that the small increase in accuracy does not justify the significant increase in computational time.

2.3.2 Random Seed Cloud Variation

Different random configurations of clouds can produce different albedos. For instance, if there are only two clouds in a particular cube, one could coincidentally be on top of the other. This would reflect significantly less light than two adjacent clouds, even if all other parameters remain the same. So, we would like to find out how much albedo variation can occur because of cloud placement variation.

By using different random seeds, we can very easily use our Monte Carlo method to generate a different simulation with the clouds in different places. Using a different random seed distributes the mass differently. In order to determine the range of results we would get for each fractal distribution, we substituted three random seeds in our routines, and the results are presented in figure 5.

The different random configurations of clouds can produce significantly different results, especially with lower fractal seeds, meaning that the clouds are thick small clouds in

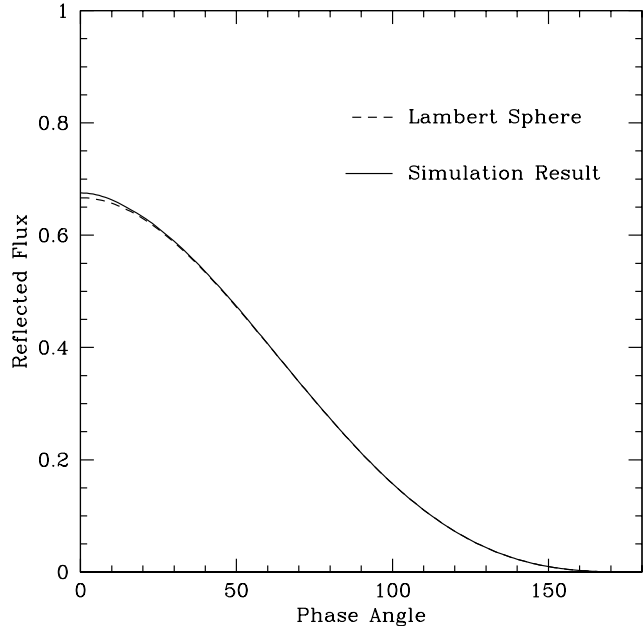


Figure 4. *Our results agree with Lambert Sphere* This graph shows a comparison of our simulation results and an independently calculated Lambert's sphere with isotropic scattering from the surface of the planet. The results are an excellent match, though the small discrepancy is caused by the coarseness of our numerical integration.

a few places instead of thinner clouds more uniformly distributed. We can see that in the most extreme case, with a fractal seed of 8, the values of reflectance can vary by up to 20% from the mean of all cases of $fs = 8$. However, in all other cases the specific values of reflectance vary by only 1-7% of the mean of each fractal seed. We can see why a smoother model can begin to give homogeneous results (which is why a fractal seed of 128 produces only 0.6-1.5% variation from the mean), but we would then expect that the fractal seed of 2 would also show significant variation. However, it seems that when the clouds are only one or two distinct entities, being close together is very unlikely. There is less of a chance for two clouds to be right on top of one another, thereby significantly changing the amount of cloud coverage and affecting the albedo.

3 SIMULATION RESULTS

3.1 Fiducial Model

We have chosen a set of fiducial models against which we will compare all other models. The fiducial models are simplistic and it is easy to understand the processes in each. Our fiducial models will have a forward throwing single scattering phase function with $h_{gg}=0.5$, an single particle albedo of 0.5, a transparent bottom layer, a smooth, uniform density atmosphere, and optical depths of 0.1, 1, 10, and 100. Figure 6 shows the four smooth models on a y-scale dependent on the Lambert sphere surface reflection.

We choose these parameters to keep our first models

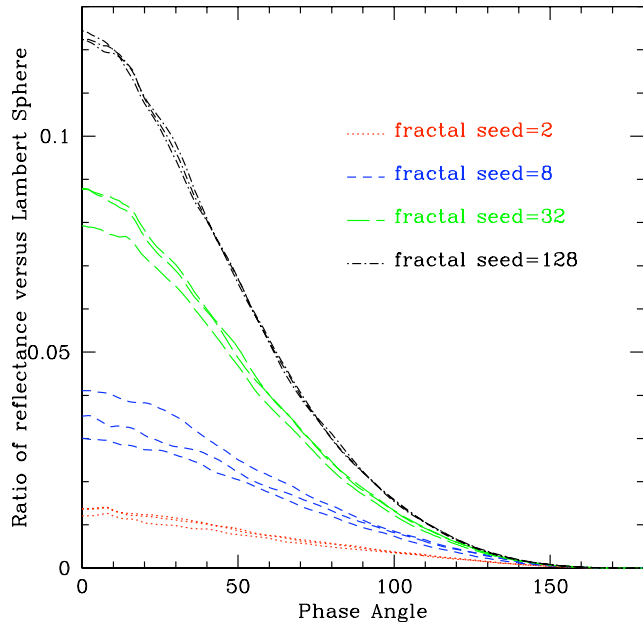


Figure 5. *Different Random Seeds show Albedo Variation.* We have run several different random seeds, in order to generate different cloud configurations and determine the variability of the albedo due to a different cloud configuration. The fractal seed = 8 shows the most significant variability (between 5 and 20%), whereas the other fractal seeds vary between 1 and 5%.

simplistic, but also to start with parameters that are similar to the values we wish to explore further. For instance, our choice for the single scattering albedo (0.5) and phase function ($h_{gg}=0.5$) are similar to values for enstatite, iron, and corundum, which are suggested condensates in extrasolar planetary atmospheres (Seager, Whitney and Sasselov 2000). The optical depths we chose to explore vary over what is reasonably expected for an exoplanet atmosphere. And though we can insert multiple species or horizontal limits on our particles, we have chosen not to, in order to keep our fiducial models as simplistic as possible.

However, even our fiducial models can reveal atmospheric trends. One thing that immediately comes to our attention is that there is a “best case” optical depth somewhere near $\tau = 10$. Lower optical depths allow too many photons through the entire grid, without reflecting them at all. For higher optical depths, too many photons are absorbed by the medium, which decreases the overall albedo. Thus, there is an optical depth “sweet spot,” at least in this fiducial model of albedo=0.5 and $h_{gg}=0.5$.

3.2 Parameter Exploration

3.2.1 Fractal Models

Figure 7 shows the results of several of our fractal models versus the fiducial smooth models of figure 6. There are several tendencies displayed in the figure’s four plots. In general, as the cloud has a higher optical depth, more photons will be scattered back out of the atmosphere, resulting in a higher planetary albedo. However, there seems to be a detri-

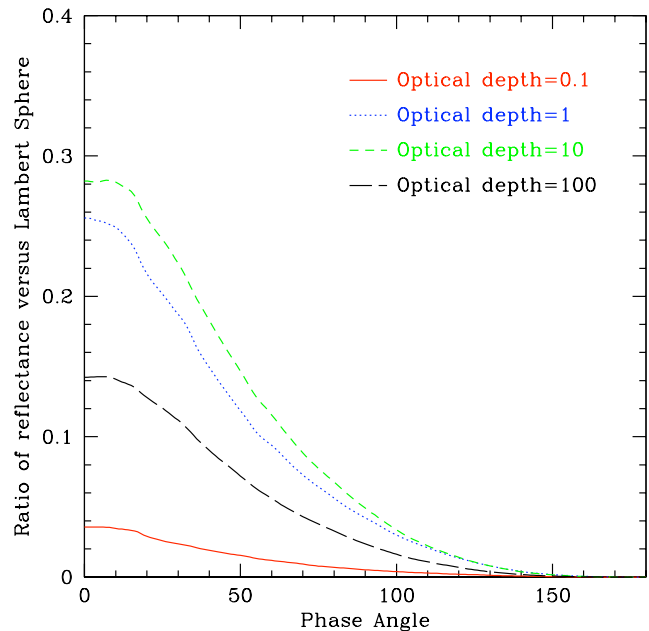


Figure 6. *Fiducial Models.* Here we display the phase functions of our fiducial set of models, which range in optical depth from 0.1 to 100. We used single scattering albedo of 0.5, single scattering phase function of $h_{gg}=0.5$, a transparent bottom layer, and a smooth uniform density atmosphere. Notice that the results are the same for any optical depth over 10.

mental effect at higher optical depths, for instance $\tau = 100$, in which the increased optical depth starts to trap more photons than it had been scattering in lower optical depth atmospheres. This is exhibited by $\tau = 10$ resulting in a higher albedo than $\tau = 100$. Photons in both cases enter the atmospheric simulation at the top of the atmosphere, traveling downward, and hit a cloud which scatters them back up. In the case of $\tau = 10$, the photons may pass through another cloud on the way out that does not have the optical depth to absorb the photon. However, in the case of $\tau = 100$, the photon is absorbed, resulting in a lower over-all albedo for the planet. This optical depth value of approximately 10 could be considered an optical depth “sweet spot,” where there is maximum scattering and thus maximum albedo. Since our varying optical depths correlate to different wavelengths, we can use this information to predict the most favorable observing wavelength for a particular atmosphere.

We also see that uniformly the smooth model produces a higher albedo than any of the fractal models. This is to be expected, since the “holes” inherent to the fractal model will let the photons in and then absorb them when they are headed out of the atmosphere.

3.2.2 FSmooth

Our value of f_{smooth} determines the percentage of mass to be used in the fractal distribution, versus what is distributed uniformly throughout the grid. For example, an f_{smooth} value of 1 will distribute all the mass uniformly throughout the grid, and none will be distributed fractally. An f_{smooth} value of 0.5 will distribute half the mass throughout the grid

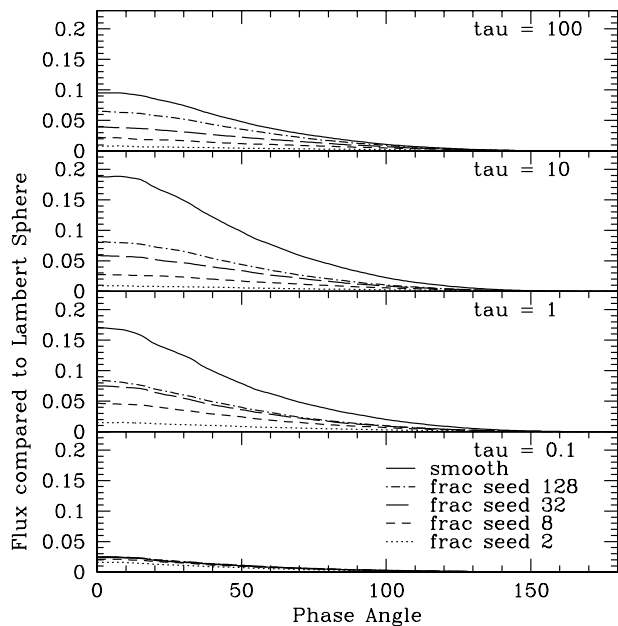


Figure 7. *Fractal Models.* Phase functions of our fractal set of models range in optical depth from 0.1 to 100. We used single scattering albedo of 0.5, a single scattering of $h_{gg}=0.5$, a transparent bottom layer, and a fractured cloud structure ranging from small dense clouds (fractal seed = 2) to thin, dispersed clouds (fractal seed = 128). Our y-scale is again compared to a Lambert sphere.

uniformly, and half will be distributed fractally. Many times we will make f_{smooth} either 100% or 0% (we actually use 10^{-6} to approximate zero, due to code limitations) to easily determine if the source of effects are the fractal distribution or something else.

We can see in figure 8 that any inclusion of a fractal distribution of mass decreases the albedo of the entire planet significantly. The completely smooth model has nearly a factor of two increase in albedo compared to *any* of the fractal models.

3.2.3 Bottom Layer or Surface

The bottom layer of our simulation represents the bottom of the atmosphere. On a rocky planet, the bottom layer should act like a surface of a rocky planet, be it snow or water or sand. On a gas giant planet, the bottom layer is a bit more nebulous, because there is no distinct stopping point. In that case we must make a best guess as to how much atmosphere we want to simulate, and how to treat the photon packets that make it through the entire (simulated) atmosphere. We can assign one of three characteristics to the bottom layer: Lambert, dense, or transparent. A Lambert surface will isotropically reflect outward all radiation incident on its surface. A dense surface is simply a very dense layer of mass, so dense that no photons will go through it. However, it differs from the Lambert surface in that it can absorb (or scatter) some photons, depending on its assigned albedo. A transparent surface allows all the photons to flow through it. The photons are then lost, as if they had all been absorbed

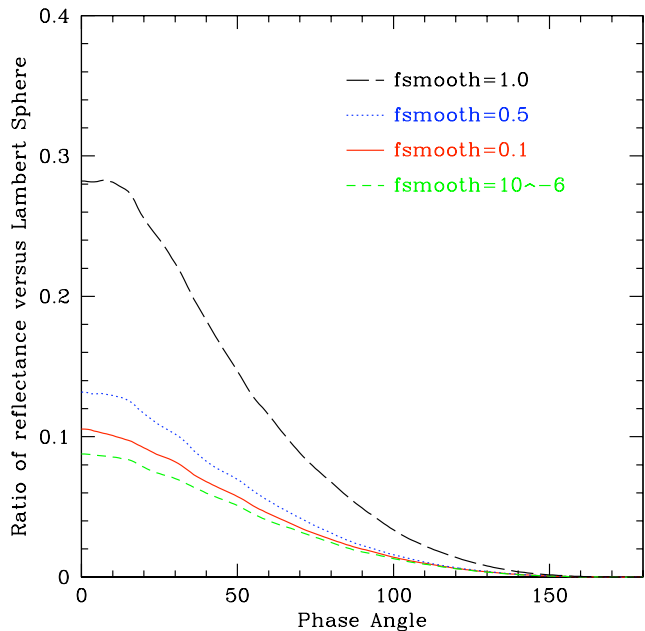


Figure 8. *FSmooth.* Phase functions of several simulations using varying f_{smooth} values. In all cases we are using $\tau = 10$ and fractal seed = 32 (90% coverage). It is apparent that any inclusion of fractal variety decreases the albedo of the entire system. Our y-scale is again compared to a Lambert sphere.

at the bottom. They do not travel to the other side of the planet and come out.

We find that when we vary the bottom layer, it can predictably make a huge impact on a subset of our models, especially those models in which sparse cloud coverage exposes most of the surface to direct contact with the photons, or in which the optical depth of the clouds is so low that the majority of the reflected light is reflected from the bottom. We find that all of these effects dissipate once the optical depth is at least equal to 10, or when a fractal seed of 32 is used, meaning that 90% of the atmosphere is covered with clouds. Figure 9 shows the pronounced effect on the sparse and low optical depth simulations.

3.2.4 Single Scattering Phase Functions

As noted previously, we can specify a particular single scattering phase function for each of the species within our simulation. We use a Henyey-Greenstein approximation to compute the phase function, and assign a specific h_{gg} value. The values of h_{gg} vary between -1 and 1 , with -1 being strongly backscattering, zero being isotropic, and 1 being strongly forward-throwing. As expected, a strongly backscattering single phase function can contribute positively to the entire albedo of the planet. Figure 10 shows that the back scattering phase contributes to a much higher albedo, but there is something funny going on. I think it is because I calculated only half of the planet's brightness and then multiplied by two. I need to go back and check that, because it seems to me like the back scattering function should be better than the isotropic function at phases less than 90° , but should be worse for phases more than 90° . That is because at some

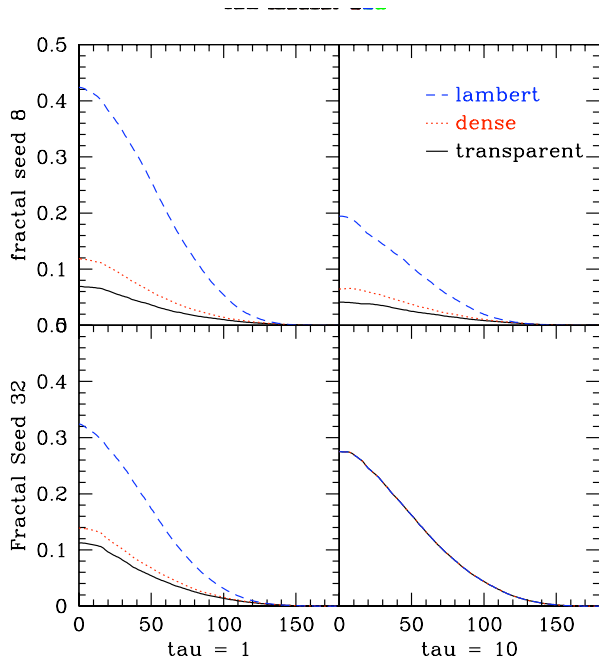


Figure 9. *Bottom Layer of Simulation.* Here we display the phase functions of several different simulations, each one using a different bottom layer. We compare two optical depths ($\tau = 1$ and $\tau = 10$) and two fractal distributions, (fractal seed = 8 [45% coverage] or fractal seed = 32[90% coverage]). It is clear that only low optical depths and sparse cloud coverage allows a significant contribution from the bottom layer.

point the back scattering should make a planet harder to see. I don't have to worry about most of my plots, though, because I used isotropic scattering, which doesn't have a "favorite" side. Thank goodness.

3.2.5 Single Particle Albedo

One of the most significant parameters we can set within the simulation is the single particle albedo, usually set to 0.5. When we set the albedo to 0.8 or 0.2, it results in a much more and much less reflective surface, respectively, as indicated in 11. This is one of the weaknesses of our code, in that we don't reprocess the light absorbed in the atmospheric medium and reemit it at a different wavelength. As stated earlier, we treat different wavelengths independently. Presumably in a medium that has a low albedo, and absorbs most of photons, a significant amount of energy would be reprocessed and reemitted.

4 DISCUSSION

Based on our simulations, several factors can significantly affect the entirety of the albedo of an extrasolar planet. Some of the factors contribute only in certain situations, while others make a significant impact in nearly every simulation.

Single scattering albedo affects the simulations more than any other parameter. This is to be expected, since we are mainly interested in the overall albedo of a planet, and it will not be highly reflective if the individual particles

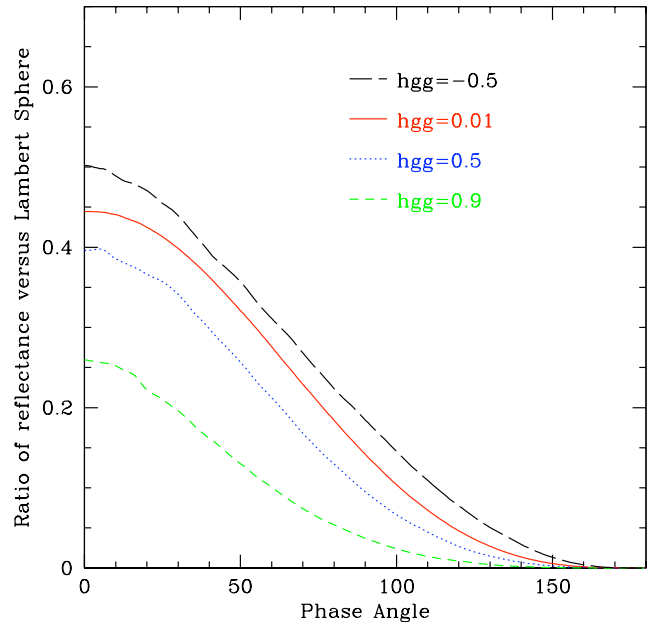


Figure 10. *Single Phase Functions.* All of these phase functions used a $\tau = 10$ and a fractal seed of 32. In most of our explorations, we used a single scattering phase function with an hgg value of 0.5. Here we compare that to isotropic scattering (hgg = 0.01), a more forward-throwing scattering phase (hgg = 0.9) or a back scattering phase (hgg = -0.5). The back scattering phase sends so much more light back out of the atmosphere that it contributes to a much larger albedo. However, I don't understand why it doesn't cross the line of the isotropic scattering around 90 degrees.

within its atmosphere aren't reflective. Certainly other elements might counteract the detrimental result of a low single scattering albedo (such as a highly backscattering phase function), but if a highly absorptive cloud layer is high in an extrasolar planetary atmosphere, then it will be very difficult to have a highly reflecting total atmosphere.

The second most important parameter which affects the total albedo of the planet is the fractal distribution of the mass. Of primary importance is fractally distributed mass. Any fractal mass will reduce the overall albedo significantly. However, overall albedo is also heavily affected by the clumpiness of the clumpy atmosphere. This is represented in our code by the fractal seed, where a low fractal seed results in a few dense clouds, and a high fractal seed results in many thinner clouds.

Immediately apparent is that the reflectivity of the atmosphere does not follow a simple function based on the amount of cloud coverage, as we can see a certain wavelengths (or optical depth of 1) a fractal seed of 128 results in the same phase curve as a smooth model, whereas at other wavelengths (optical depth of 100) the same fractal seed gives 20% lower albedo than the smooth model. The structure of the mass throughout the atmosphere is important, and affects the albedo significantly. We can see that a certain amount of cloud coverage is necessary to significantly impact the overall albedo, as the fractal seed of 2 (cloud coverage of ~15% shows).

The optical depth also has a significant impact on the

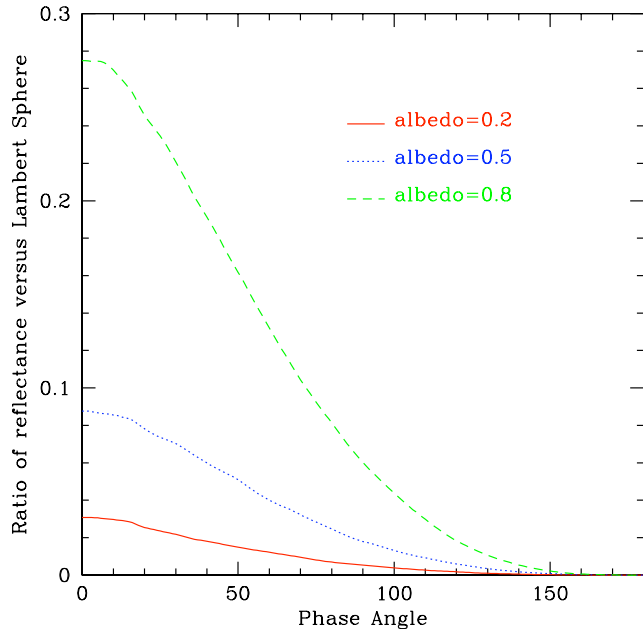


Figure 11. *Single Albedos.* All of these phase functions used a $\tau = 10$ and a fractal seed of 32. In most of our explorations, we used an albedo of 0.5. Here we compare that to two other albedos, 0.8 and 0.2. The lower albedos make the planet as a whole much less reflective, as the photon packets are essentially absorbed.

overall albedo of a planet, but it is tied to the fractal models intimately, because of the way we calculate optical depth. As mentioned earlier, the optical depths assigned to a fractal model are the optical depths of an equivalent smooth model. So, when we generate a simulation with a fractal seed of 2 and optical depth of 10, we are putting all the mass that would generate $\tau = 10$ in the entire grid into two large, dense clouds. These clouds individually might have optical depths of 100.

In particular the optical depth affects the fractal models in a way it does not affect the smooth models. The smooth models, lacking any internal structure, have ceilings to their reflectivities, reached around $\tau = 10$, after which higher optical depths decrease the overall reflectivity. In those higher optical depth cases, the photons are forced into the simulation because of a forward scattering phase function, and then are more likely to be absorbed by the medium.

In the fractured cases there are pockets of low density, in which photons travel deep into the simulation grid, and then are scattered. In these cases, the photons are not scattered back in exactly the way they came in, but instead in a different way which takes them into a cloud, only to be eventually absorbed. This lowers the overall albedo and is unique to the structures with three-dimensionality.

Single scattering phase functions also affect the total reflectivity, but not consistently in a positive or negative way. In the situation of a phase angle of zero, or when the planet is in phase “full planet,” a strongly back-scattering single phase function will contribute to a much higher albedo. However, when the planet is at a 90° phase angle, the back scattering will cause more of the scattered photons to head back to the parent star, instead of in our direction. For this rea-

son the single scattering phase function is significantly, but only in limited situations.

Similarly, the choice of a bottom layer affects a subset of simulations, but not all. Only when the optical depth of a simulation is low enough to allow most photons to pass through the atmosphere, or when the fractal seed is low enough that there is generally very little cloud coverage will the bottom layer significantly affect the overall albedo. To an extent, both conditions must be true, as shown in figure 9. However, in some real planetary situations this is the case, for instance on Mars, so it cannot be completely discounted as a contributor to planetary albedo.

5 CONCLUSIONS

Our Monte Carlo-based radiation transfer simulations offer a powerful tool to simulate extrasolar planetary atmospheres. The various parameters allow us to build a realistic model of an atmosphere based on the most current predictions of extrasolar planet atmospheric composition. Our code is sufficiently flexible that it could also be used to simulate atmospheres within our solar system, for example on Jovian moons, and with some modification could be useful even in an Earth context.

We have been unable, heretofore, to view reflected starlight scattered from the surface of an extrasolar planet. We know the planets’ sizes and emperis to a precision that if they were reflective, we would have detected them. Thus, we must build models to better understand why these extrasolar planet atmospheres are so dark. The fractal characteristic of clouds, which can only be explored in a three-dimensional model like ours, and which strongly affects the albedo of a planet, could help explain this darkness.

ACKNOWLEDGEMENTS

Ben Hood would like to thank the Marshall Commission and the Department for Terrestrial Magnetism of the Carnegie Institution of Washington for financial support.

REFERENCES

- Brown, T.M., Charbonneau, D., Gilliland, R.L., Noyes, R.W., & Burrows, A. 2001, *ApJ*, 552,699
- Charbonneau, D., Noyes, R., Korzennik, S., Nisenson, P., Jha, S., Vogt, S., Kibrick, R., 1999, *ApJ*, 522, L145
- Charbonneau, D.; Allen, Lori E.; Megeath, S. Thomas; Torres, Guillermo; Alonso, Roi; Brown, Timothy M.; Gilliland, Ronald L.; Latham, DavidW.; Mandushev, Georgi; O’Donovan, Francis T.; Sozzetti, Alessandro, 2005, *ApJ*, 626, 523
- Cameron, Andrew Collier, Horne, K., Penny, A., James, D., 1999, *Nature*, 402, 751
- Cameron, Andrew Collier; Horne, K., James, D., Penny, A., Semel, M., 2001, in Penny, A., Artymowicz, P., Lagrange, A.M., Russell, S., eds, *Proc. IAU Symp. 202, Planetary Systems in the Universe. A.S.P.*, San Francisco.
- Deming, Drake; Seager, Sara; Richardson, L. Jeremy; Harrington, Joseph, 2005, *Nature*, 434, 740
- Elmegreen, Bruce G., 1997, *ApJ*, 477, 196

- Kuchinke, C., Fienberg, K., Nunez, M., 2004, *Journal of Applied Meteorology*, 43, 751
- Leigh, C., Cameron, A.C., Horne, K., Penny, A., James, D., 2003, *MNRAS*, 344, 1271
- Lovejoy, S., 1982, *Science*, 216, 185
- Rowe, J.F., Matthews, J.M. Seager, S., Kuschnig, R. Guenther, D.B., Moffat, A.F.J., Rucinski, S.M., Sasselov, D.D., Walker, G.A.H., Weiss, W.W., 2006, *ApJ*, (in publication)
- Sánchez, N., Alfaro, E., Pérez, E., 2005, *ApJ*, 625, 849
- Seager, S., Whitney, B., Sasselov, D.D., 2000, *ApJ*, 540, 504
- Sobolev, V.V., *Light Scattering in Planetary Atmospheres*, Pergamon Press, New York, 1975
- Sudarsky, D., Burrows, A., Hubeny, I., Li, A., 2005, *ApJ*, 627, 520
- Wood, Kenneth, Reynolds, R.J., 1999, *ApJ*, 525, 799
- Wood, K., Haffner, L. M., Reynolds, R. J., Mathis, J. S., Madsen, G., 2005, *ApJ*, 633, 295